# Molecular Orientation of Langmuir−Blodgett Films of Designed Heme Protein and Lipoprotein Maquettes

**Xiaoxi Chen, Christopher C. Moser, Denis L. Pilloud, and P. Leslie Dutton***

*Johnson Research Foundation, Department of Biochemistry and Biophysics, University of Pennsylvania, Philadelphia, Pennsylvania 19104*

*Received: April 14, 1998; In Final Form: June 9, 1998*

*De novo* designed tetra-α-helical heme proteins $(\alpha ss\alpha)_2$, comprising two identical helix-loop-helix subunits, αssα, were immobilized as monolayer films on solid substrate using the Langmuir−Blodgett (LB) technique. These LB heme protein films were characterized by circular dichroism (CD), ultraviolet−visible (UV−vis), and Fourier transformed infrared (FTIR) spectroscopy. During the formation of monolayer films on substrate, the $(\alpha ss\alpha)_2$ heme proteins dissociate into their αssα subunits, but remain α-helical and retain the bis-histidine heme ligation. The α-helices are oriented in the film close to parallel to the substrate plane and the heme macrocycle planes are tilted at 40°. There is no detectable ordering of the molecules in the plane of the monolayer. However, when the loop region was palmitoylated to confer amphiphilic character to the heme proteins, a profound change of state at high surface pressure was displayed. Transfer of this high-pressure film onto solid substrate also generates a film with α-helices near 0° and hemes planes at 40°, but with added order: remarkably the α-helices and one heme edge assume a strong orientation parallel to the direction of withdrawal of the substrate from the LB subphase.

## Introduction

A major barrier to understanding the molecular design of natural redox proteins is their great structural complexity which arises from the multiple roles that protein structure have evolved in native biological systems. *De novo* design and synthesis of proteins is a relatively new approach aimed to minimize complexity[1] and facilitate focus on a particular aspect of protein assembly, structure, dynamics, or catalysis. In this regard we are working to identify the engineering behind the assembly of proteins incorporating redox cofactors[2] that gives rise to highly directed long-range electron transfer in oxidoreductase enzymes. Several species of water-soluble tetra-α-helical bundle proteins which accommodate hemes and other natural cofactors have been designed and synthesized as molecular "maquettes" of electron-transfer proteins in nature.[2,3] These simplified synthetic heme proteins have proven to possess characteristic electronic and optical properties of the kind familiar in natural heme proteins.

*De novo* design and synthesis affords great freedom to modify these proteins to control interactions between these α-helices and engineer the assembly of the proteins on surfaces. Surface studies facilitate the exploration of the factors that govern biological electron tunneling and long-range electron transfer,[4,5] and also form the foundations for engineering molecular wires, novel biosensor design, and bioelectronic development.[6,7]

The Langmuir−Blodgett (LB) technique has been extensively used to order and immobilize natural electron-transfer proteins on solid surfaces.[8−10] The technique includes several advantages not available in solution studies: (1) A protein monolayer at air−water interface can be transferred after establishing a molecular organization of the film selected at different surface pressure or surface density, (2) a protein monolayer formed at air−water interface can be transferred to many different surfaces, including those prepared for electrodic studies, (3) protein multilayers can be obtained by repeating the monolayer transfer process as many times as desired, and (4) the transferred film can be studied in different environments such as air or solution. We have explored the LB film properties of two related synthetic heme protein maquettes: (1) A highly water soluble tetra-α-helical bundle heme protein which is based on the prototype described by Robertson et al.,[2] slightly modified only to improve packing of the bundle interior.[3] A pair of identical α-helices are linked by a disulfide bond at their cysteinyl N-termini to make an αssα subunit. Two αssα subunits spontaneously assemble in aqueous solution to form a tetra-α-helical bundle $(\alpha ss\alpha)_2$ with stripes of charged glutamates and lysines on the outside of a hydrophobic core, as shown in Figure 1A. (2) A lipoprotein $(palm_2\text{-}\alpha ss\alpha)_2$ variant obtained by palmitoylating the $(\alpha ss\alpha)_2$ heme protein in the loop region, as shown in Figure 1B.

The success of the LB technique draws on the property of amphiphilic molecules when spread and compressed at air−water interface to form a compact monolayer with hydrophobic and hydrophillic parts directed to air and water, respectively. When this technique is applied to nonamphiphilic water-soluble proteins, difficulties can be encountered. Simple water-soluble proteins at the air−water interface tend to expose their hydrophobic interior to the air, causing dramatic changes of their native structure which may be detrimental to the function of the proteins or even cause the liganded cofactors to dissociate from the protein. Although our tetra-helix-bundle heme protein is highly water soluble, we anticipated that it could retain its α-helical and heme ligating structure at air−water interface

* To whom correspondence should be addressed. FAX: (215) 573-2235. E-mail: dutton@mail.med.upenn.edu.

S1089-5647(98)01855-0 CCC: $15.00 
Published on Web 07/29/1998

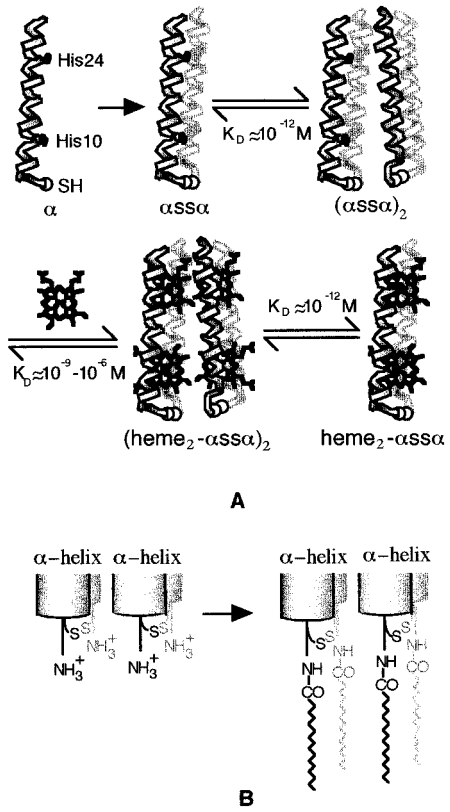


**Figure 1.** Working model of the heme protein maquettes construction. (A) The construction of $(heme_2\text{-}\alpha ss\alpha)_2$: Solid-phase peptide synthesis produced the 31-amino acid peptide, α, which is oxidized to form a dihelix unit, αssα. Two αssα units self-assemble into a tetra-helix-bundle, $(\alpha ss\alpha)_2$. The tetra-helix-bundle coordinates hemes by bis-histidyl ligation to form the heme protein maquette, $(heme_2\text{-}\alpha ss\alpha)_2$. The dissociation constant of $(heme_2\text{-}\alpha ss\alpha)_2$ into its subunits, $heme_2\text{-}\alpha ss\alpha$, is very small in aqueous solution. (B) The construction of lipoprotein maquette by palmitoylation of the heme protein maquette in the loop region.

because it can simply dissociate into its dihelix subunits (Figure 1A) to expose the hydrophobic "interior" to the air, while maintaining the exterior charges in contact with water. The lipoprotein variant was intended to confer amphiphilicity to water-soluble tetra-helix-bundle heme protein so that when compressed at air−water interface it might promote a dominating exposure of the hydrophobic tails to the air while retaining an intact tetra-helix-bundle assembly in the water subphase. Thus, we expected the two maquettes to display two different kinds of molecular order at the air−water interface as well as after immobilization on the substrate.

The first stage of this study describes the properties of the proteins at the air−water interface and the spectral probes of secondary structure and heme environment in LB films. The second stage describes the determination of the orientation of the heme protein maquettes on solid substrate, which underlies any prospective inquiries into the functional properties of the heme protein maquette LB film such as electron tunneling and surface oxidation−reduction catalysis. Linear dichroism of the ligated heme absorption spectrum is a well-established way to determine the average angle between the normal of the heme plane and the normal of the substrate surface of heme protein films.[11−13] Linear dichroism of the amide dipole transitions[14−17] and oriented circular dichroism[18−20] have been commonly used to determine the average angle between the α-helix axis and substrate surface.

## Materials and Methods

**Maquette Design.** The four helix bundles were the same α-helix sequence as described by Gibney et al.[3]:

Ac−CGGGEIWKLH EEFLKKFEEL LKLHEERLKK L-$CONH_2$

Two of the 31-amino acid peptides were linked by a disulfide bond at their cysteinyl N-termini to form αssα.[2,3] These αssα units self-assemble in aqueous solution into a tetra-α-helical bundle $(\alpha ss\alpha)_2$, which can adopt a clear syn- or anti-topology with S-S loops at the same or opposite ends of the bundle, depending on sequence and cofactor binding.[21] Figure 1A shows a syn- topology. Histidines are present for a bis-histidine ligation at four sites within the tetra-helical bundles. For the lipoprotein, the two N-amino termini of each αssα were used to form amide bonds with palmitic acid (Figure 1B) or cholanic acid.[22]

**Chemicals and Solvents.** Palmitic acid, diisopropylcarbodiimide, trifluoroacetic acid (TFA), and dimethyl sulfoxide (DMSO) were purchased from Aldrich Chemical Co. (Milwaukee, WI). Ethanedithiol and 1-hydroxy-benzotriazol were purchased from Fluka (Ronkonkoma, NY). Fmoc-protected amino acid perfluorophenyl esters were purchased from PerSeptive Biosystems (Framingham, MA) with the exception of Fmoc-L-Arg(Pmc)-OPfp, which was obtained from Bachem (King of Prussia, PA). NovaSyn PR-500 resin was purchased from Calbiochem-Novabiochem (La Jolla, CA). All other chemicals and solvents were reagent grade. Water was purified using a Milli-Q water system from the Millipore Corp. (Bedford, MA).

**Peptide Synthesis.** The peptides were synthesized on a continuous-flow Milligen 9050 solid-phase synthesizer using standard Fmoc/tBu protection strategy with NovaSyn PR-500 resin at 0.2-mmol scale. The side-chain protecting groups used were as follows: Lys(tBoc), Glu(OtBu), Cys(Trt), and Arg(Pmc). The N-terminus was either acetylated (1:1 (v/v) acetic anhydride−pyridine for 30 min) for the heme protein maquette or attached to palmitic acid for the palmitoylated heme protein maquette as described below. The peptides were cleaved from the resin and simultaneously deprotected using 90:8:2 trifluroacetic acid−ethanedithiol−water for 2 h. Crude peptides were precipitated and triturated with cold ether, dissolved in water (0.1% TFA), lyophilized, and purified to homogeneity by reversed-phase C18 HPLC using aqueous acetonitrile gradients containing 0.1% (v/v) TFA. The resulting peptide identities were confirmed with laser desorption mass spectrometry.

**Peptide Palmitoylation.** Palmitic acid was attached to the N-terminus of the 31-amino acid peptide on a fraction of the resin using a 5-fold excess of palmitic acid, diisopropylcarbodiimide, *N*,*N*-diisopropylethylamine, and 1-hydroxybenzotriazole. After 2 h, the resin was thoroughly washed with *N*,*N*-dimethylformamide (DMF) and dried before cleavage and purification as described above.

**Heme Protein Preparation.** The 31-amino acid peptides were dissolved in 100 mM ammonium hydrogen carbonate buffer (pH 9.2) in air to allow the cysteines to oxidize to form the 62-amino acid peptide αssα. After 4 h the solution was frozen and lyophilized. When needed, the αssα peptides were dissolved in phosphate buffer (50 mM phosphate, 100 mM NaCl, pH 8.0) to yield a final concentration of 0.01 mM $(\alpha ss\alpha)_2$. The solutions of heme proteins were prepared according to the procedure reported by Robertson et al.[2] Heme was incorporated into $(\alpha ss\alpha)_2$ to form $(heme_2\text{-}\alpha ss\alpha)_2$ from a stock solution of 5 mM of Fe(III) protoporphyrin IX (heme) in DMSO, by

successive additions of 0.1 heme per binding site until 1 heme/bis-his site was reached. During each addition, the solution was well stirred and then allowed to equilibrate for 5 min. The final concentration of DMSO in the aqueous solution was always lower than 1:200 (v:v). The heme incorporation was monitored by the increase of the Soret band maximum, between 410 and 412 nm ($e$ = 120,000 $M^{-1}$ $cm^{-1}$).

The palmitoylated 31-amino acid peptides were dimerized to palm$_2$-αssα, and heme was incorporated into (palm$_2$-αssα)$_2$ in a similar way. However, it was clear that only 2 hemes of the 4 heme binding sites can be incorporated into each (palm$_2$-αssα)$_2$. A possible source for this limitation may be that the one or more C16 tails fold into the hydrophobic core of (palm$_2$-αssα)$_2$ in solution and consequently sterically hinder the histidines at position 10 near the N-termini. In contrast, heme binding to the histidines at position 24 is not hindered.

**Langmuir Film Preparation and Isotherm Measurement.** A Langmuir−Blodgett film balance (Lauda Filmbalance FW2, Sybron/Brinkmann, Westbury, NY) was used to make the films following the general procedure described elsewhere.[23] The aqueous subphase contained 1 mM phosphate at pH 8.0. All films were made under an argon atmosphere at a subphase temperature of 10 °C. Proteins were spread at the air−water interface using the "glass-rod" method.[24] This involved placing a 0.6 mm diameter glass rod at a small angle (<30°) relative to the trough plane, just touching the water surface, to which 2-mL aliquots of material were added every 10−15 s. During this procedure the trough surface area was held constant. Surface pressure/area isotherms were measured using a barrier speed of 10 $cm^2$/min.

**Substrate Preparation.** Quartz slides, 1 mm in thickness (Esco Products, Oak Ridge, NJ), were sonicated first in detergent solution and then in water. This was followed by immersion in fresh NOCHROMIX acid (0.5 M of ammonium persulfate in concentrated sulfuric acid) at room temperature for about 2 h. They were then thoroughly rinsed with water, and finally stripped of visible surface water with a stream of argon. $CaF_2$ windows (International Crystal Labs, Garfield, NJ) were cleaned with chloroform. The cleaned slides and windows were used immediately.

**Langmuir−Blodgett Monolayer Film Preparation.** Proteins were spread as discussed above, compressed, and held at constant surface pressure. The slide or window was first passed vertically into the subphase at a relatively fast speed (800 mm/min), sufficient to prevent detectable depositions of peptides as indicated by the absence of a change in the film area. The submerged slide was then withdrawn slowly through the surface at 5 mm/min. Multilayers could be built up by repeating the process.

**Circular Dichroism Spectropolarimetry.** Circular dichroism spectra were measured in an Aviv 62DS circular dichroism spectropolarimeter. The quartz slides coated with LB film were positioned in the instrument using a homemade slide holder and oriented perpendicularly to the incident measuring beam. A baseline reference was recorded by using a blank, cleaned quartz slide.

**UV−vis Absorption Spectroscopy and Linear Dichroism.** UV−vis absorption spectra were recorded with a Perkin-Elmer UV−vis spectrophotometer Lambda 2. The quartz slides coated with LB film were positioned in the instrument using a homemade slide holder. The holder allowed the slides to be oriented at any desired angles with respect to the incident measuring beam. For linear dichroism measurements, a UV dichroic polarizer from Oriel Corporation (Stratford, CT) sensitive from 230 to 770 nm was placed between the incident beam and the coated slide. In all cases a baseline reference was recorded by using a blank, cleaned quartz slide.

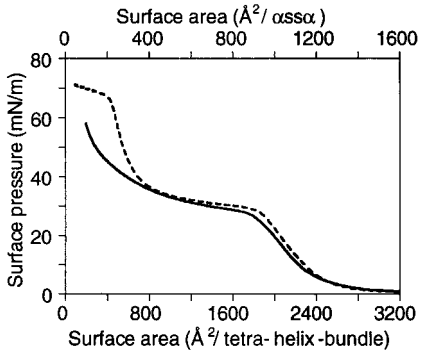


**Figure 2.** Surface pressure−area isotherms of the monolayer films derived from (heme$_2$-αssα)$_2$ (solid line) and (heme-palm$_2$-αssα)$_2$ (dashed line).

**FTIR Spectroscopy and Linear Dichroism.** IR spectra were collected using a Bruker IFS66 Fourier transform infrared spectrometer. Data collection parameters were set for 2 $cm^{-1}$ resolution and 512 scans were collected for both film sample and background spectra. Linear polarization of the IR signal beam was accomplished using an IR polarizer of 0.12-mm-wide strips of aluminum on a KRS-5 substrate (Graseby/Specac). $CaF_2$ windows coated with LB film were positioned in a specially designed holder which oriented the film normals at any desired angles with respect to the signal beam. Each sample file was carefully referenced to a film-free substrate background spectrum of the appropriate polarization.

## Results

**1. The Heme Protein Maquettes on Air−Water Interface.** The pressure−area isotherms in Figure 2 gave the first indication of the molecular orientation of the heme protein maquettes at the air−water interface. The isotherms of both (heme$_2$-αssα)$_2$ and (heme-palm$_2$-αssα)$_2$ show an inflection point at approximately 1900 Å$^2$/tetra-helix-bundle, indicating the transition from gaseous state to liquid expanded state of the monolayer. In the low surface pressure gaseous state, the surface pressure will depend on the number of independent particles at the surface, and a two-dimensional version of the ideal gas law applies:[25]

$$\pi (A - A_0) = k\,T/n \qquad (1)$$

where $\pi$ is the surface pressure, $A$ is the surface area per protein molecule, $A_0$ is the limiting area per molecular, $k$ is the Boltzmann constant, $T$ is the temperature in degrees Kelvin, and $n$ is the number of molecules associated as independent particles. Fitting eq 1 to the gaseous state region of the (heme$_2$-αssα)$_2$ monolayer isotherm (from 1 to 5 mN/m) yields $n$ = 0.47, $A_0$ = 2370 Å$^2$/tetra-helix-molecule. The fit is similar for the (heme-palm$_2$-αssα)$_2$ monolayer, yielding $n$ = 0.55, $A_0$ = 2390 Å$^2$/tetra-helix-molecule. The values of $n$ which are close to 0.5 in both cases indicate that the tetra-helix-bundle in solution dissociates into independent αssα subunits at the air−water interface. The scale for area per subunit, Å$^2$/αssα, is shown as the top $x$-axis in Figure 2.

The value of $A_0$ (approximately 1190 Å$^2$/αssα-subunit for monolayers derived from both maquettes) was in agreement with the modeled molecular area of the αssα units when the two helices lie parallel to the interface side by side. This is about 5-fold the molecular area that the αssα units would occupy if

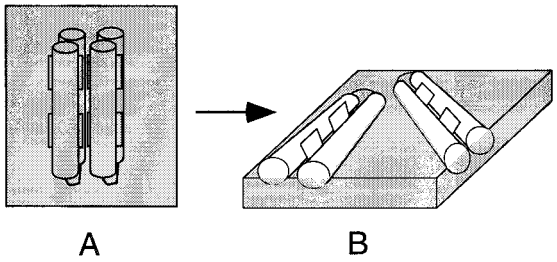


**Figure 3.** Models of heme protein maquette assembly. (A) The heme protein maquette assumes a tetra-helix-bundle assembly in aqueous phase. (B) The tetra-helix-bundle dissociates into the dihelical subunits at air−water interface.

the two helices stood perpendicular to the interface. These observations strongly suggest that the independent subunits heme$_2$-αssα and heme-palm$_2$-αssα lie flat at the air−water interface (Figure 3).

When the film is compressed beyond the inflection point at 950 Å$^2$/αssα, the surface pressure increases only to a small extent per unit decrease of surface area for both heme$_2$-αssα and heme-palm$_2$-αssα subunits, which corresponds to the liquid expanded state of the film. However, when compressed below 300 Å$^2$/αssα, the film of heme-palm$_2$-αssα behaves markedly differently from that of heme$_2$-αssα. The surface pressure of heme-palm$_2$-αssα film increases steeply from 35 mN/m to 67 mN/m when the film was compressed from 300 to 200 Å$^2$/αssα, where at 200 Å$^2$/αssα another inflection point is encountered. In contrast the surface pressure of heme$_2$-αssα film increases continuously until the limit of compression without displaying another inflection point.

The inflection point at 200 Å$^2$/αssα of the heme-palm$_2$-αssα film should correspond to the collapse point of the film. The 200 Å$^2$ value is significant because it closely corresponds to the molecular area of heme-palm$_2$-αssα when the helices are all perpendicular to the air−water interface and thus is the minimal area to hold a monolayer of heme-palm$_2$-αssα. Thus, in contrast to the heme$_2$-αssα film, it seems that the heme-palm$_2$-αssα film undergoes a phase transition to the condensed state in the range of 300−200 Å$^2$/αssα. This can be explained by the more amphiphilic nature of the palmitylated heme protein maquette, which may promote the reorientation of the heme-palm$_2$-αssα film at the high surface pressure.

**2. Structural Conservation of the Heme Protein Maquettes on LB Films.** *UV−vis Spectra.* Figure 4A compares the UV−vis absorption spectra of the (heme$_2$-αssα)$_2$ protein maquette on LB film and in solution. It is clear that both absorption spectra are almost identical. All of them display the characteristic UV−vis absorption properties of bis-histidine hemes and hence it is evident that the bis-histidine heme ligation is conserved on the LB film. This is also the case for the (heme-palm$_2$-αssα)$_2$ protein maquette (not shown): again the UV−vis absorption spectra on LB film and in solution are identical, and are the same as those shown in Figure 4A.

*CD Spectra.* Figure 4B compares the CD spectra of the (heme$_2$-αssα)$_2$ protein maquette on LB film and in solution. The CD spectrum of the LB film conserves the shape that is characteristic of a predominately α-helical structure. The CD spectra of the (heme-palm$_2$-αssα)$_2$ protein maquette on LB film and in solution (not shown) are the same as those shown in Figure 4B. We note, however, that the ratio of two minima at 208 and 222 nm of the LB film spectrum differs from that of the solution spectrum; we will return to this later.

*FTIR Spectra.* The conservation of the α-helical secondary structure was also confirmed by the FTIR absorption spectra

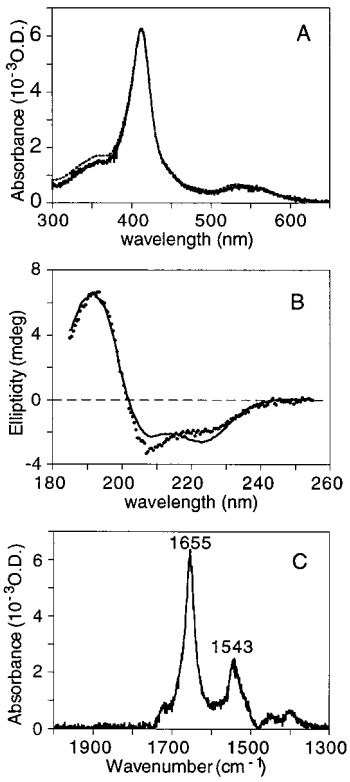


**Figure 4.** Spectroscopy of the heme protein maquette in solution and on LB film. (A) UV−vis absorption spectra of (heme$_2$-αssα)$_2$ on LB film (monolayer on quartz slide) (solid line) and in solution (50 mM phosphate, 100 mM NaCl, pH 8.0) (dashed line). The solution spectrum has been normalized to the Soret band (411 nm) of the film absorption spectrum. (B) CD spectra of (heme$_2$-αssα)$_2$ on LB film (5-layer on quartz slide) (filled circles) and in solution (50 mM phosphate, 100 mM NaCl, pH 8.0) (solid line). The solution spectrum has been normalized to the band at 192 nm of the film CD spectrum. (C) FTIR absorption spectrum of a 5-layer (heme$_2$-αssα)$_2$ LB film on $CaF_2$ window.

of the LB film. The correlation between the frequency of the amide I vibrational mode and the nature of the secondary structure has been well established in the literature. An amide I band in the frequency range of 1650−1660 cm$^{-1}$ is characteristic of α-helical structure, but extended $\beta$-structure generally produces peaks in the 1630−1640 cm$^{-1}$ and 1670−1690 cm$^{-1}$ ranges.[26] Both α-helical structure and unordered structure may produce amide I peaks near 1650 cm$^{-1}$, but the full width at half-height of the band (FWHH) is significantly narrower for α-helical structure compared to unordered structure.[27] As seen in Figure 4C, the amide I mode of the (heme$_2$-αssα)$_2$ protein maquette on LB film contains a highly symmetrical band centered at 1655 cm$^{-1}$ with a FWHH of 28 cm$^{-1}$, indicative of a high helical content. The peak near 1544 cm$^{-1}$ which corresponds to the amide II mode has a noticeable shoulder which we suspected may be due to superposition of multiple modes. The FTIR spectrum of the (heme-palm$_2$-αssα)$_2$ protein maquette on LB film (not shown) is indistinguishable from the spectrum shown in Figure 4C.

**3. Orientation of the Heme Protein Maquettes on LB Films.** The dichroic ratio of absorption of IR or UV−vis light linearly polarized perpendicular vs parallel to the plane of incidence is the key parameter used in the analysis of the molecular orientations in films. Figure 5 illustrates the general arrangement of a linear dichroism experiment. The $x-y$ axes represent the plane of the substrate or the LB film, the $x-z$ axes represent the plane of incidence of the incoming light, and $\theta$ is the incident angle. The dichroic ratio for a band, $D$, is

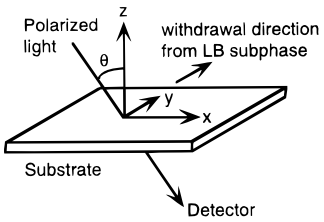


**Figure 5.** Experimental arrangement of a linear dichroism measurement.

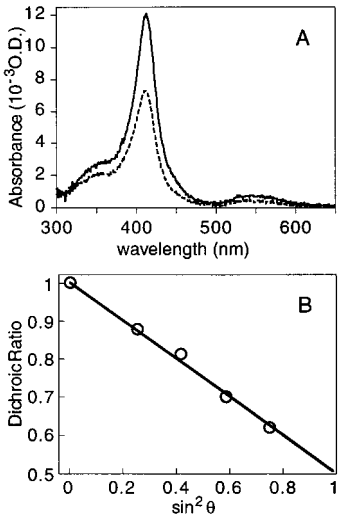


**Figure 6.** UV−vis linear dichroism of heme$_2$-αssα LB film. (A) Absorption spectra of a monolayer LB film on quartz slide (transferred at 20 mN/m) with parallel (dashed line) and perpendicular (solid line) polarized incident measuring light. The incident angle is 60°. (B) The dependency of dichroic ratio on $\sin^2\theta$.

defined as the ratio of absorption for radiation polarized parallel ($A_{||}$) and perpendicular ($A_\perp$) to the plane of incidence:

$$D = \frac{A_{||}}{A_\perp} = \frac{\mu_x^2 E_x^2 + \mu_z^2 E_z^2}{\mu_y^2 E_y^2} \tag{2}$$

where $E_x$, $E_y$, and $E_z$ are the components of electric field vector and $\mu_x^2$, $\mu_y^2$, and $\mu_z^2$ are the components of the square of the transition dipole moments or absorption coefficients in the coordinate system as shown in Figure 5. For perpendicularly polarized light, $E_y^2 = E_0^2$, and for parallel polarized light, $E_x^2 = E_0^2 \cos^2\theta$, $E_y^2 = E_0^2 \sin^2\theta$. So

$$D = \frac{\mu_x^2}{\mu_y^2}\cos^2\theta + \frac{\mu_z^2}{\mu_y^2}\sin^2\theta \tag{3}$$

When the protein film possesses cylindrical symmetry about the normal to the substrate plane (z-axis), we have $\mu_x^2 = \mu_y^2$. In this case the dichroic ratio is expected to be linearly dependent on $\sin^2\theta$ with no dichroism ($D = 1$) at $\theta = 0$:

$$D = 1 + \left(\frac{\mu_z^2}{\mu_y^2} - 1\right)\sin^2\theta \tag{4}$$

*UV−vis Linear Dichroism.* Figure 6A shows the UV−vis absorption spectra of a monolayer LB film of di-heme-αssα with parallel and perpendicular polarized incident light and with an incident angle of 60°. Figure 6B shows the dependency of dichroic ratio on $\sin^2\theta$ for the monolayer LB film of di-heme-αssα. The measured dichroic ratios fall on a line as predicted.

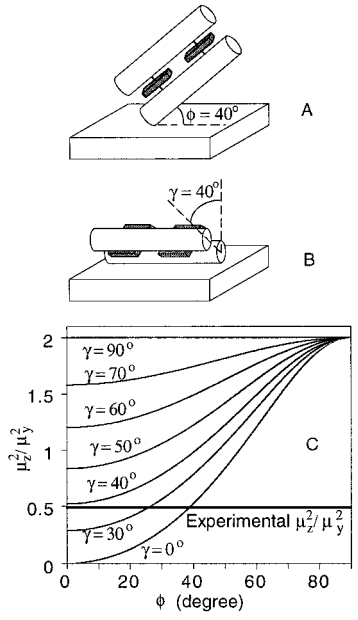


**Figure 7.** Molecular orientation of heme$_2$-αssα LB film on solid substrate. (A) and (B) Two possible orientations consistent with the UV−vis linear dichroism results. But only the orientation shown in (B) is also consistent with the FTIR linear dichroism results. (C) The thin lines describe $\mu_z^2/\mu_y^2$ as a function of $\phi$ at different $\gamma$ values according to eqs 6 and 7. The thick line is the experimental value of $\mu_z^2/\mu_y^2$.

The dichroic ratio is 1 at 0° incidence which agrees with the cylindrical symmetry assumption; thus, there is no preferred orientation in the $x-y$ plane ($\mu_x^2 = \mu_y^2$). The extrapolated value of dichroic ratio at 90° incidence reflects $\mu_z^2/\mu_y^2$, the ratio of the square of the out-of-plane and the in-plane dipole moments. This value will be used in the following analysis.

It is generally assumed that the electronic transitions responsible for the Soret and α-bands in hemes are isotropically polarized in the plane of the heme.[28] A formula has been proposed[11] to estimate the average orientation of the heme group in heme proteins.

$$D = \cos^2\theta + \frac{2\sin^2\psi}{1+\cos^2\psi}\sin^2\theta \tag{5}$$

where $\psi$ is the angle between the normal of the heme plane and the normal of the substrate plane. Using this expression, the angle $\psi$ is determined to be 40°. In the heme protein maquette, bis-histidine ligation constrains the heme plane to be approximately parallel to the α-helical axis. Figure 7 shows two extreme helical geometries consistent with $\psi = 40°$. Figure 7A illustrates a geometry where the α-helices are tilted 40° with respect to the substrate and the plane containing the helices is normal to the substrate; in Figure 7B the helices are parallel to the substrate, and the plane containing the helices is rotated 40° from the normal-to-substrate position. If we let $\phi$ be the angle between helices and the substrate, and $\gamma$ be the rotation angle of the plane containing the helices relative to the normal-to-substrate position, we can derive the following expressions for $\mu_x^2$, $\mu_y^2$, and $\mu_z^2$:

$$\mu_x^2 = \mu_y^2 = \frac{1}{2}(1+\cos^2\phi) - \frac{1}{2}\cos^2\phi\sin^2\gamma \tag{6}$$

$$\mu_z^2 = \sin^2\phi + \cos^2\phi\sin^2\gamma \tag{7}$$

The dichroic ratio is

$$D = \cos^2\theta + \frac{\sin^2\phi + \cos^2\phi\sin^2\gamma}{\frac{1}{2}(1+\cos^2\phi) - \frac{1}{2}\cos^2\phi\sin^2\gamma}\sin^2\theta \quad (8)$$

In the cases when $\gamma = 0°$ (the plane containing the helices is normal to substrate) or $\phi = 0°$ (helices parallel to the substrate plane), this formula of dichroic ratio simplifies to eq 5.

Figure 7C shows $\mu_z^2/\mu_y^2$ plotted as a function of $\phi$ at different $\gamma$ values according to eqs 6 and 7. The experimental value of $\mu_z^2/\mu_y^2$ obtained from Figure 6B is drawn as a line. Only $\phi$ values less than 40° are consistent with the measured dichroism, with $\gamma$ increasing from 0° to 40° as $\phi$ decreases to zero.

*FTIR Linear Dichroism.* FTIR was used as a complement of UV−vis linear dichroism to determine the heme protein maquette orientation. Figure 8 shows an example of an FTIR linear dichroism. The FTIR absorption spectra shown is of a 5-layer LB film of heme$_2$-αssα with parallel and perpendicular polarized incident light and with an incident angle of 60°.

Here we let $\omega$ be the angle between the amide I transition dipole and the helix axis, and $\phi$ is still the angle between the helix axis and substrate plane. Assuming that the amide I transition dipole is cylindrically symmetric about the α-helix axis, we can derive the following expressions of $\mu_x^2$, $\mu_y^2$, and $\mu_z^2$:

$$\mu_x^2 = \mu_y^2 = \cos^2\phi + \frac{1}{4}(3\sin^2\phi - 1)\sin^2\omega \quad (9)$$

$$\mu_z^2 = \sin^2\phi - \frac{1}{2}(3\sin^2\phi - 1)\sin^2\omega \quad (10)$$

The dichroic ratio is

$$D = \cos^2\theta + \frac{\sin^2\phi - \frac{1}{2}(3\sin^2\phi - 1)\sin^2\omega}{\cos^2\phi + \frac{1}{4}(3\sin^2\phi - 1)\sin^2\omega}\sin^2\theta \quad (11)$$

In Figure 9, the experimental value of $\mu_z^2/\mu_y^2$ obtained from FTIR linear dichroism of the LB film of heme$_2$-αssα is used to determine the possible range of $\phi$ and $\omega$ in a similar way as the UV−vis linear dichroism. $\mu_z^2/\mu_y^2$ is plotted as a function of $\phi$ at different $\omega$ values according to eqs 9 and 10. The measured value of $\mu_z^2/\mu_y^2$ for the amide I mode in the spectra of heme$_2$-αssα film is plotted as a line.

The orientational distributions of the amide I transition moments in α-helical polypeptides are not yet clearly determined. The reported literature values for the average orientation of the transition moment of the amide I mode with respect to the principle helix axis range from 27 to 40°.[29] If we take the literature average value of $\omega$ to be 34°, then the $\phi$ angle determined from the measured value of $\mu_z^2/\mu_y^2$ is zero, corresponding to Figure 7B. As shown in Figure 9, our data do not support a $\omega$ greater than 34°. Using the reported lower extreme of $\omega = 27°$, the $\phi$ angle cannot exceed 14°.

**4. Special Orientation of the Palmitylated Heme Protein Maquette on LB Films.** LB films of heme-palm$_2$-αssα prepared at both low (20 mN/m) and high (45 mN/m) surface pressures have the same average out-of-plane to in-plane UV−vis and FTIR dichroic ratios ($\mu^2_{\text{out-of-plane}}/\mu^2_{\text{in-plane}} = \mu_z^2/(1/2\ \mu_y^2 + 1/2\ \mu_x^2)$) as heme$_2$-αssα LB films discussed in the previous section, indicating a similar orientation of individual molecules with respect to the substrate. Surprisingly, when transferred at high surface pressure (45 mN/m), LB films of heme-palm$_2$-αssα show dichroism that is conspicuous even at 0° incidence (Figure 10A). Defining the *y*-axis as in the plane of the substrate and parallel to the direction of withdrawal of the slide from LB subphase, and the *x*-axis as in the plane of the substrate and perpendicular to the direction of withdrawal (Figure 5), eq 3 can be fit to the dichroic ratios at different incident angles to give $\mu_x^2/\mu_y^2 = 0.7$, $\mu_z^2/\mu_y^2 = 0.44$, and $\mu_z^2/\mu_x^2 = 0.63$. Absorbance is maximal in the *y* direction (Figure 10B).

Figure 11 summarizes the orientation of the heme protein maquettes with and without C16 appendages transferred to

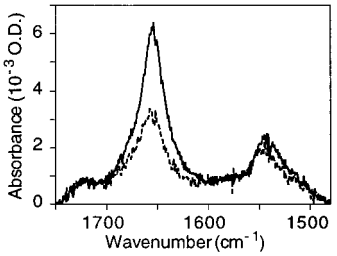


**Figure 8.** FTIR linear dichroism of heme$_2$-αssα LB film. Absorption spectra of a 5-layer LB film on $CaF_2$ window (transferred at 20 mN/m) with parallel (dashed line) and perpendicular (solid line) polarized incident light. The incident angle is 60°.

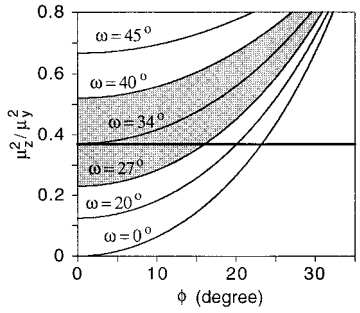


**Figure 9.** Analysis of FTIR linear dichroism. The thin lines describe $\mu_z^2/\mu_y^2$ as a function of $\phi$ at different $\omega$ values according to Eqs 9 and 10. The thick line is the experimental value of $\mu_z^2/\mu_y^2$. The shaded region indicates the range of the $\omega$ values reported in the literature.

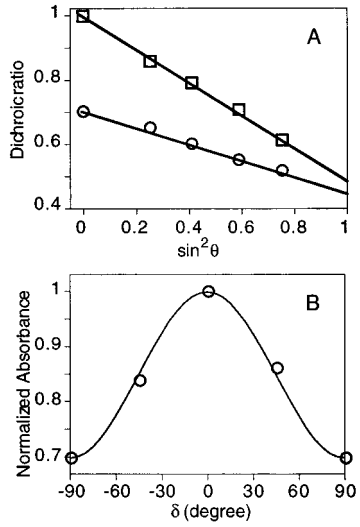


**Figure 10.** Linear dichroism of the palmitylated heme protein maquette on LB film. (A) Dependency of UV−vis absorption dichroic ratio ($D$) on $\sin^2\theta$. Squares: LB film of heme-palm$_2$-αssα transferred at low surface pressure (20 mN/m). Circles: LB film of heme-palm$_2$-αssα transferred at high surface pressure (45 mN/m). (B) Normalized absorbance as a function of $\delta$, the angle between the direction of incident light polarization and the direction of substrate withdrawal. Circles: measured data. Solid line: the data are fitted with the function $(1-0.3\ \sin^2\delta)$.

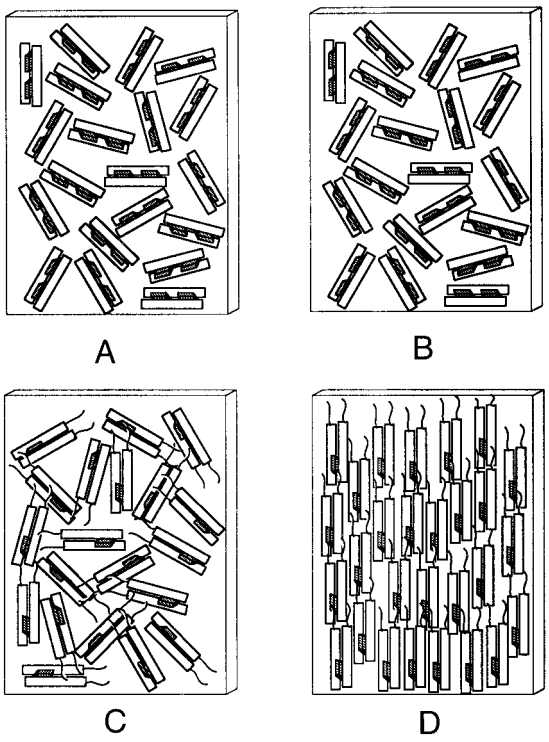


**Figure 11.** Illustration of the molecular orientations on LB film. (A) LB film of heme$_2$-αssα transferred at low surface pressure. (B) LB film of heme$_2$-αssα transferred at high surface pressure. (C) LB film of heme-palm$_2$-αssα transferred at low surface pressure. (D) LB film heme-palm$_2$-αssα transferred at high surface pressure.

substrate at low and high surface pressure. In all cases the α-helices are approximately parallel to the substrate, and the planes of hemes are tilted 40° with the substrate plane. In most cases the direction of the α-helices in the $x-y$ plane appear random, but at high pressure those with C16 appendages have α-helices approximately aligned in the $y$-direction—the direction of substrate withdrawal. In this case, the substrate coated with LB film behaves like a polarizer itself. The dichroic ratios $\mu_x^2/\mu_y^2 = 0.7$ and $\mu_z^2/\mu_y^2 = 0.44$ are close to an ideal case in which the α-helices and one heme edge are perfectly aligned in the $y$-direction and the heme plane normal is 40° from the substrate normal, for which $\mu_x^2/\mu_y^2 = \cos^2 40° = 0.59$ and $\mu_z^2/\mu_y^2 = \sin^2 40° = 0.41$. This tells us that if the film comprised two populations, one with helices oriented in the $y$ direction and one in the $x$ direction, then 85% of the α-helices would be oriented in the $y$ direction. Dichroism in the plane of substrate was also seen in the infrared amide I absorption ($\mu_x^2/\mu_y^2 = 0.9$). This in-plane dichroism is measured with multilayer films (for good IR signal-to-noise ratio) and appear less well aligned than the monolayer films used for UV−vis studies.

## Discussion

Our results indicate that both heme protein maquette and palmitoylated heme protein maquette lie flat with the α-helices parallel to the air−water interface when they are spread and equilibrated at low surface pressure. The hydrophobic−hydrophilic interface apparently encourages the tetrα-helix-bundle in solution to disassemble into its dihelix subunits to maintain the charged polar sides of each helix in contact with water while the hydrophobic sides face the air. Nevertheless, the α-helices of each dihelix subunit continue to bis-histidine ligate the hemes. Other amphiphilic α-helical peptides have been found before to lie flat at the air−water interface.[30,31]

The in-plane orientation of α-helices after transfer onto solid substrate is proved by UV−vis and FTIR linear dichroism. This orientation also helps to explain the noticeable difference in ratio of the 208 and 222 nm CD peaks in the film relative to solution. Just such CD ratio changes have been observed in systems with oriented α-helices.[18−20] For example, de Jongh et al.[20a] modeled CD spectra of α-helix parallel and perpendicular to incident beam by deconvoluting the polylysine CD spectra in terms of Gaussian absorption bands. The modeled CD spectrum of α-helix perpendicular to the incident beam (parallel to the substrate surface) shown in Figure 1 of ref 20a is very similar to the CD spectrum of our LB film shown in Figure 4B. This observation further supports the results derived from UV−vis and FTIR linear dichroism. But caution must be taken in analyzing the tilt angle of the α-helices based on the CD spectra, because other factors such as the loss of coiled-coil tertiary structure may also contribute to the change of the ratio of the 208 and 222 nm CD peaks in the film relative to solution.

Films of the palmitoylated heme protein when sufficiently compressed seem to regain tetra-α-helix-bundle assembly at the air−water interface and reorient with the α-helices perpendicular to the interface. The supporting evidence includes: (1) The phase transition at the high-pressure part of isotherm of the palmitoylated heme protein suggests that the molecules at air−water interface undergo reorientation; (2) the surface area per dihelix subunit at this high-pressure transition (200−300 Å$^2$) is about the size of the molecule when the helices are perpendicular to the air−water interface; (3) the thickness of the film under these conditions measured by X-ray reflectivity experiments is also consistent with the length of long axis of the molecule.[32] However, it is clear that when the palmitoylated heme protein maquette is transferred from the air−water interface to a substrate surface it lies flat even when it is transferred at high surface pressure. The orientations of individual molecules with respect to the substrate were observed to be similar in all cases, suggesting that they are essentially governed by the interaction between the molecules and substrate surface during and after the transfer process. Rearrangement of molecular orientations is commonly found in LB transfer processes. For example, studies of fatty acid salts by Zasadzinski and co-workers[33] indicate that the structure of the transferred films often bears no resemblance to that present at the air−water interface and may instead depend quite strongly on the structure of the substrate.

The extra order of palmitoylated heme protein maquette on the substrate surface seems to arise from the perpendicularly oriented molecules in the film at air−water interface. The forces associated with transfer to substrate probably have tilted the helices down toward the substrate and establish the special in-plane alignment of palmitoylated heme protein maquette on LB film. Similar orientations have been found for phthalocyanine polymer LB film, the molecules of which are aligned parallel to the direction of substrate withdrawal.[34] It is believed that the order was introduced during LB deposition, probably at the meniscus, where shear forces are maximized.[34,35] Another similar situation was observed for behenic acid LB film on graphite where the molecules were found by scanning tunneling microscopy to rearrange to form an oriented monolayer parallel to the substrate, although they were perpendicular to the air−water interface before transfer.[36,37]

In conclusion, LB film of heme protein maquettes and lipoprotein maquettes were constructed with well-defined molecular orientations. A special in-plane molecular order was

found for lipoprotein maquette LB film. Such high ordering is very important for applications such as constructing molecular wires on a surface coated with spatially separated electrodes. We note too that palmitoylation is not a rare phenomenon in native biological systems. Many membrane-associated proteins such as insulin receptor of human lymphocytes, transferrin receptor of human T cell line, and rhodopsin of retina are palmitoylated posttranslationally. Because the palmitoylation in native biological systems is believed to be involved in membrane anchorage,[38−40] it may be reasonable to expect that palmitoylation of heme protein maquettes will help anchor these synthetic molecules at membrane-water interfaces.

**Acknowledgment.** This research was supported by grant from NIH GM41048 and in part MERSEC/IRG grant from NSF (DMR91-20668). We also thank Dr. Francesc Rabanal, Dr. Brian R. Gibney, and Dr. Ronald W. Visschers for the many stimulating discussions.

## References and Notes

(1) DeGrado, W. F.; Wasserman, A. R.; Lear, J. D. *Science* **1989**, *243*, 622−628.

(2) Robertson, D. E.; Farid, R. S.; Moser, C. C.; Urbauer, J. L.; Mulholland, S. E.; Pidikiti, R.; Lear, J. D.; Wand, A. J.; DeGrado, W. F.; Dutton, P. L. *Nature* **1994**, *368*, 425−432.

(3) Gibney, B. R.; Rabanal, F.; Skalicky, J. J.; Wand, A. J.; Dutton, P. L. *J. Am. Chem. Soc.* **1997**, *119*, 2323−2324.

(4) (a) Pilloud, D. L.; Rabanal, F.; Moser, C. C.; Dutton, P. L. *Biophys. J.* **1998**, *74*, No. 2, Pt. 2, A250, W.-PM-N2. (b) Pilloud, D. L.; Rabanal, F.; Gibney, B. R.; Farid R. S.; Moser, C. C.; Dutton, P. L. *J. Phys. Chem. B* **1998**, *102*, 1926−1937.

(5) Armstrong, F. A.; Heering, H. A.; Hirst, J. *Chem. Soc. Rev.* **1997**, *26*, 169−179.

(6) Nicolini, C. *Biosens. Bioelectron.* **1995**, *10*, 105−127.

(7) Jortner, J.; Ratner, M. A., Eds. *Molecular Electronics*; Blackwell Science: London, 1997.

(8) Pepe, I. M.; Nicolini, C. *J. Photochem. Photobiol. B* **1996**, *33*, 191−200.

(9) (a) Alegria, G.; Dutton, P. L. *Biochim. Biophys. Acta* **1991**, *1057*, 239−257. (b) Alegria, G.; Dutton, P. L. *Biochim. Biophys. Acta* **1991**, *1057*, 258−272.

(10) Moser, C. C.; Sension, R. J.; Szarka, A. Z.; Repinec, S. T.; Hochstrasser, R. M.; Dutton, P. L. *Chem. Phys.* **1995**, *197*, 343−354.

(11) Blasie, J. K.; Erecinska, M.; Samuels, S.; Leigh, J. S. *Biochim. Biophys. Acta* **1978**, *501*, 33−52.

(12) Pachence, J. M.; Amador, S.; Maniara, G.; Vanderkooi, J.; Dutton, P. L.; Blasie, J. K. *Biophys. J.* **1990**, *58*, 379−389.

(13) (a) Edmiston, P. L.; Lee, J. E.; Wood, L. L.; Saavedra, S. S. *J. Phys. Chem.* **1996**, *100*, 775−784. (b) Edmiston, P. L.; Lee, J. E.; Cheng, S. S.; Saavedra, S. S. *J. Am. Chem. Soc.* **1997**, *119*, 560−570.

(14) Jang, W.-H.; Miller, J. D. *J. Phys. Chem.* **1995**, *99*, 10272−10279.

(15) Axelsen, P. H.; Kaufman, B. K.; McElhaney, R. N.; Lewis R. N. A. H. *Biophys. J.* **1995**, *69*, 2770−2781.

(16) Arkin, I. T.; Russ, W. P.; Lebendiker, M.; Schuldiner, S. *Biochemistry* **1996**, *35*, 7233−7238.

(17) Boncheva, M.; Vogel, H. *Biophys. J.* **1997**, *73*, 1056−1072.

(18) Olah, G. A.; Huang, H. W. *J. Chem. Phys.* **1988**, *89*, 2531−2538.

(19) Wu, Y.; Huang, H. W.; Olah, G. *Biophys. J.* **1990**, *57*, 797−806.

(20) (a) de Jongh, H. H. J.; Goormaghtigh, E.; Killian, J. A. *Biochemistry* **1994**, *33*, 14521−14528. (b) de Jongh, H. H. J.; Brasseur, R.; Killian, J. A. *Biochemistry* **1994**, *33*, 14529−14535.

(21) Gibney, B. R., unpublished results.

(22) Cholanic acid [17-$\beta$-(1-methyl-3-carboxypropyl)etiocholane] is a natural compound structurally similar to cholesterol. Lipoprotein maquettes with cholanic acid and C16 appendage behave similarly in many aspects, especially their isotherms at air−water interface are similar. We have chosen the lipoprotein maquette with C16 appendage as the main subject of our experiments.

(23) (a) Popovic, Z. D.; Kovacs, G. J.; Vincett, P. S.; Alegria, G.; Dutton P. L. *Chem. Phys.* **1986**, *110*, 227−237. (b) Popovic, Z. D.; Kovacs, G. J.; Vincett, P. S.; Alegria, G.; Dutton P. L. *Biochim. Biophys. Acta* **1986**, *851*, 38−48.

(24) Trurnit, H. J. *J. Colloid Interface Sci.* **1960**, *15*, 1−13.

(25) Adamson, A. W.; Gast, A. P. *Physical Chemistry of Surfaces*, 6th ed., John Wiley & Sons: New York, 1997; Chapters 2, 4.

(26) Braiman, M. S.; Rothschild, K. J. *Annu. Rev. Biophys. Biophys. Chem.* **1988** *17*, 541−570, and references therein.

(27) Venyaminov, S. Y.; Kalnin, N. N. *Biopolymers* **1990**, *30*, 1259−1271.

(28) Adar, F. In *The Porphyrins*; Dolphin, D., Ed.; Academic Press: New York, 1978; Vol. III, 167−206.

(29) Goormaghtigh, E.; Cabiaux, V.; Ruysschaert, J. M. *Subcell. Biochem.* **1994**, *23*, 329−362, and references therein.

(30) DeGrado, W. F.; Lear, J. D. *J. Am. Chem. Soc.* **1985**, *107*, 7684−7689.

(31) Fujita, K.; Kimura, S.; Imanishi, Y. *Langmuir* **1995**, *11*, 1675−1679.

(32) Strzalka, J.; Chen, X.; Moser, C. C.; Dutton, P. L.; Ocko, B. M.; Blasie, J. K. *Biophys. J.* **1998**, *74*, No. 2, Pt. 2, A236, W.-PM-D2.

(33) Zasadzinski, J. A.; Viswanathan, R.; Madsen, L.; Garnases, J.; Schwartz, D. K. *Science* **1994**, *263*, 1726−1733.

(34) Orthman, E.; Wegner, G. *Angew. Chem., Int. Ed. Engl.* **1986**, *25*, 1105.

(35) Ulman, A. *An Introduction to Ultrathin Organic Films From Langmuir−Blodgett to Self-Assembly*; Academic Press: San Diego, CA, 1991; Chapter 2.

(36) Kuroda, R.; Kishi, E.; Yamano, A.; Hatanaka, K.; Matsuda, H.; Eguchi, K.; Nakagiri, T. *J. Vac. Sci. Technol. B* **1991**, *9*, 1180−1183.

(37) Kishi, E.; Matsuda, H.; Kuroda, R.; Takimoto, K.; Yamano, A.; Eguchi, K.; Hatanaka, K.; Nakagiri, T. *Ultramicroscopy* **1992**, *42−44*, 1067−1072.

(38) Towler, D. A.; Gordon, J. I. *Annu. Rev. Biochem.* **1988**, *57*, 69−99.

(39) Schmidt, M. F. G. *Biochim. Biophys. Acta* **1989**, *968*, 411−426.

(40) Mcllhenney, R. A. J. *TIBS* **1990**, *15*, 387−391.